An extension to classical lamination theory for use with functionally graded plates

R.G. Reid*

R. Paskaramoorthy

DST/NRF Centre of Excellence in Strong Materials and RP/Composites Facility
School of Mechanical, Industrial and Aeronautical Engineering
University of the Witwatersrand, Johannesburg
Private Bag 3, Wits 2050, South Africa

Abstract

An extension to classical lamination theory is presented for the improved analysis of thin to moderately thick functionally graded plates. The method results in an explicit formulation that accommodates any through-thickness variation in the elastic, hygrothermal and piezoelectric properties of each layer. Additionally, variations in the material rotation angle, temperature, moisture content and electric field strength through each layer are taken into account. The method relies on representing with polynomial series the variation in both the properties of each ply and the hygrothermal and piezoelectric loading. Validation problems are presented that demonstrate the application and accuracy of the method.

Key words: Analysis, Functionally graded materials, Lamination theory

1. Introduction

A functionally graded material is a two-part composite wherein the relative abundance of each constituent progressively changes. There are no abrupt changes in the resulting material properties and so stress concentrations within the material are eliminated. The material can consequently withstand very se-

*Corresponding author
Email addresses: robert.reid@wits.ac.za (R.G. Reid)

vere service conditions. Functionally graded materials were first proposed as a means of withstanding extreme temperature gradients in thermal barriers [1, 2]. Since then, they have been considered for wear resistant linings [3, 4, 5, 6], joining dissimilar materials [7, 8], orthopaedic [9, 10] and dental [11] implants and even as a means of reducing electrical field peaks in switchgear [12].

Many potential applications of functionally graded materials are inherently two-dimensional and so considerable effort has been directed towards the analysis of functionally graded plates (FGPs). Three-dimensional solutions are the most accurate and a number of solutions of this type are available in the literature. Reddy and Cheng [13] have presented an asymptotic analysis of a rectangular FGP subjected to transverse pressure and thermal loading. The through-thickness variation in the volume fractions of the two constituent materials was varied according to a power law. Kashtalyan [14] has obtained an elasticity solution to the problem of a transverse load acting on a plate with Young's modulus exponentially graded in the thickness direction and constant Poisson's ratio. She has also extended this work to a sandwich panel with an exponentially graded Young's modulus in the core [15]. Zenkour [16] has obtained an elasticity solution for a simply supported FGP with transverse loading and with Lamé coefficients exponentially graded. Vel and Batra [17, 18, 19] have used power series to obtain solutions for simply supported FGPs with a power-law variation in volume fraction of the constituents. Steady state thermal stresses [17], transient thermal stresses [18] and both free and forced vibrations [19] are considered in these contributions. Pan [20] has obtained exact solutions, expressed in terms of a formalism that resembles the Stroh formalism, for a simply supported plate, comprised of multiple functionally graded, anisotropic plies. The elastic properties of the individual plies are assumed to vary exponentially in the thickness direction. Recently, Alibeigloo [21] has used Fourier series and the state-space method to find an exact solution for the thermo-elastic response of FGPs with material properties that vary exponentially through the thickness but with the Poisson's ratio held constant. Amongst other results, a comparison is made with the results of Reddy and Cheng [13]. Since the

problem presented by these authors has a varying Poisson's ratio however, the results are very slightly different.

Since plates are inherently two-dimensional, it is possible to improve the computational efficiency of their analysis by reducing the problem to two dimensions. Simplifications are made in this process, however, and some loss in accuracy is inevitable. A great many two-dimensional theories have been developed that aim to minimize both computational effort and errors relative to three-dimensional solutions. These theories can be broadly broken into the equivalent single layer (ESL) and layer-wise (LW) approaches.

The ESL approach describes the displacements within a plate using mathematical functions in terms of the through-thickness coordinate. This approach has two advantages; the number of solution variables is independent of the number of layers within the plate, and continuity of displacements is automatically satisfied at the interface between layers. Since continuity of strain is, however, also satisfied at these locations, classical ESL models violate interlaminar equilibrium of the transverse stresses [22, 23].

The simplest ESL theory, referred to as the first-order shear deformation theory (FSDT), assumes a constant shear strain through the thickness and so a shear correction factor, which is problem specific, is required to account for the strain energy of shear deformation. Despite this deficiency, FSDT has been widely used in the analysis of FGPs [24, 25, 26, 27]. Third and higher-order shear deformation theories represent the out-of-plane shear stresses by a quadratic and higher order polynomials respectively, and require no shear correction factors. The third-order shear deformation theory (TSDT) has been employed in the analysis of FGPs by Reddy [24] and Ferreira *et al.* [28, 26, 29]. The latter authors made use of meshless collocation methods based on multiquadric radial basis functions. A fifth-order theory that includes deformations normal to the plate has been presented by Qian and Batra [30] and used to study transient thermoelastic deformations in a thick FGP.

Trigonometric functions can be used instead of polynomial functions to describe the through-thickness shear deformations. A sinusoidal variation allows

traction-free boundary conditions on the surfaces to be satisfied. This approach has been favoured by Zenkour for the analysis of FGPs [31, 16] and functionally graded sandwich plates [32, 33]. The latter results were compared against those obtained using both FSDT and TSDT.

Classical ESL methods cannot take account of the fact that the slope of the displacement field is discontinuous in the through-thickness direction at every interface between layers. It is possible to improve the accuracy of these analysis methods by forcing such a discontinuity in slope. To achieve this effect, a zig-zag distribution which changes direction at each layer interface is superposed on the classical in-plane displacement field. This approach has been used in the analysis of functionally graded beams [34, 35, 36] and was extended to functionally graded sandwich plates by Icardi [37]. The approach assumes that the magnitude of the zig-zag displacement remains constant through the thickness of the laminate but it has been shown to be layer-dependent [38].

The layer-wise (LW) approach was proposed to overcome the problem associated with describing the discontinuous slope of the displacement field [38]. A different set of displacement functions is used for each layer within the plate. Enforcement of continuity conditions ensures that displacement, but not strain, compatibility occurs at each interface. Interlaminar equilibrium of transverse stresses is therefore enabled. Since the number of variables depends on the number of layers, however, LW approaches can be computationally expensive. They have been extensively used in the analysis of laminated plates but seem to have found less acceptance for the analysis of FGPs, possibly because large changes to material properties can be obtained without the need for any interfaces.

Mixed formulations of both the ESL and LW approaches make use of a set of mathematical equations to describe the transverse stresses within each layer in addition to those describing the displacement. The system of governing equations is determined by means of the Reissner Mixed Variational Theorem (RMVT) rather than the Principle of Virtual Displacement (PVD). Interlaminar continuity of the transverse stresses is enforced through boundary conditions and so interlaminar equilibrium is ensured. As a consequence, a RMVT

approach is generally more accurate than a PVD approach utilizing the same order shear deformation theory [23]. Additionally, since the mixed layerwise approach furnishes a quasi-three-dimensional description of the transverse stresses, higher order versions of this approach are generally the most accurate [22]. A third-order theory of this sort has been presented for use with FGPs by Pai and Palazotto [39].

The unified formulation (UF) of Carrera [40, 41, 42] enables a large variety of plate theories to be handled in a unified manner. ESL and LW theories of any order can be considered using either PVD or RMVT formulations. The UF has been used to compare the results predicted by a number of different theories based on the RMVT [43] and PVD [44] approaches for transversely loaded FGPs. Similarly loaded functionally graded sandwich plates have been considered using both RMVT and PVD approaches [45]. Thermal loading of FGPs has been treated using the PVD approach [46]. The UF has also been extended to consider functionally graded piezoelectric plates in both sensor and actuator configurations [47]. In all of these works, the variation in through-thickness material properties is described by a combination of Legendre polynomials.

Although considerable effort has been expended in formulating plate theories that are able to efficiently deal with the non-planar deformations associated with transverse shear strains, such capabilities are not always necessary, or even desirable, when analysing FGPs. Most functionally graded materials are manufactured from refractory ceramics and metals and have transverse and in-plane moduli of the same order of magnitude. As a consequence, the transverse shear strains in FGPs are lower than those in laminated composite plates in which the transverse moduli are significantly lower those in the plane. Errors associated with neglecting these deformations in FGPs only therefore become apparent in comparatively thick plates. Additionally, the computational overhead associated with calculating the non-planar deformations is not desirable in situations, such as the analysis of thin plates, where through-thickness loading can be neglected. Interestingly, it has even been shown by Carrera [38, 48] that first order ESL theories (including those that account for normal strains, zig-zag ef-

fects and interlaminar equilibrium) give significantly less accurate estimations of the transverse shear stresses and total transverse deflection of a thin plate subjected to a linear through-thickness temperature distribution than do theories such as the classical lamination theory (CLT).

As a consequence, there is still a valid use for theories which assume that plane sections remain plane and that do not account for transverse normal strains. A range of these methods have been used to analyse the thermal stresses in infinite functionally graded plates. These include the methods of Giannakopoulos *et al.* [49], Hsueh and Lee [50], Becker *et al.* [51], Ravichandran [52] and Finot *et al.* [53]. CLT, and modifications thereof, have also been used to study this problem by Cho and Oden [54], Tsukamoto [55] and Shaw [56]. CLT has also been used to study functionally graded piezo-laminates by Taya *et al.* [57] and Almajid *et al.* [58]. The latter authors also compared the in-plane stresses calculated using CLT with those of a two-dimensional elasticity analysis of a functionally graded piezo-laminate under cylindrical bending [59]. The results obtained using the two different methods were indistinguishable for a plate aspect ratio of 75. Surprisingly, CLT still provided a reasonable representation of the in-plane stress at an aspect ratio as low as four.

Although CLT has been widely applied in the analysis of thin FGPs, it cannot directly accommodate material properties that progressively change. What is done in practice, therefore, is to discretize the plate in the thickness direction into a number of layers and then use a constant set of material properties appropriate to each layer. As a consequence, there is a discontinuity in material properties at the interface between layers which results in corresponding discontinuities in the calculated in-plane stresses. Such effects can be minimized by increasing the number of layers used in the analysis, but it is more desirable to use an approach that incorporates variation in material properties and hence allows results to be obtained directly. This paper presents such a technique. It is formulated as an extension to CLT and accommodates any through-thickness variation in material properties, hygrothermal loading and piezoelectric loading.

The actual through-thickness variations in the material properties, tempera-

ture, moisture content and electric field strength within each layer are approximated by polynomial series. Depending on the order of the series, it is possible to very accurately represent the true variation in these parameters. This approach has significant advantages. Firstly, the resulting mathematical problem can be explicitly formulated irrespective of the actual variation in material properties and loading. Secondly, the hygrothermal and piezoelectric loading are precisely represented. This is significant in view of Carrera's [48] demonstration that the use of an accurate theory can be negated if the temperature profile is not properly represented. Thirdly, the method also inherently accommodates situations where the material properties are experimentally determined and some scatter in these measurements is unavoidable. It is worth remembering that any manufacturing process used to make components from a functionally graded material (FGM) only approximates the desired variation in material properties. There is thus no point in relentlessly pursuing a solution that uses a particular mathematical function to describe the variation in material properties when a polynomial series approximation can be substituted for the same function with negligible loss of accuracy.

2. Lamination theory

Since CLT is well established, only brief details germane to the task will be given here. An interested reader is referred to the many excellent textbooks such as those of Herakovich [60] and Kaw [61] for additional details. This work introduces some new variables in addition to the familiar terms of CLT and they are defined in context.

The configuration of the laminate under consideration is illustrated in Fig. 1. It is assumed that the laminate consists of N layers of FGM possessing orthotropic material properties in the plane of the laminate. These properties, and the rotation angle of the principal material coordinate system, of each layer can vary throughout its thickness. The thickness of layer n is denoted by h_n, and that of the entire laminate by h. The z-axis, perpendicular to the plane, is taken

as positive downwards and has its origin at the mid-plane of the laminate. The z-coordinate of the mid-plane of layer n is denoted by $\bar{z}_n$. A non-dimensional measure of z is introduced within each layer such that it varies from -1 at the top surface to +1 at the bottom surface. The non-dimensional coordinate within layer n is termed Z_n.

The relationship between z and Z_n is defined as

$$z = \bar{z}_n + \frac{h_n}{2} Z_n \tag{1}$$

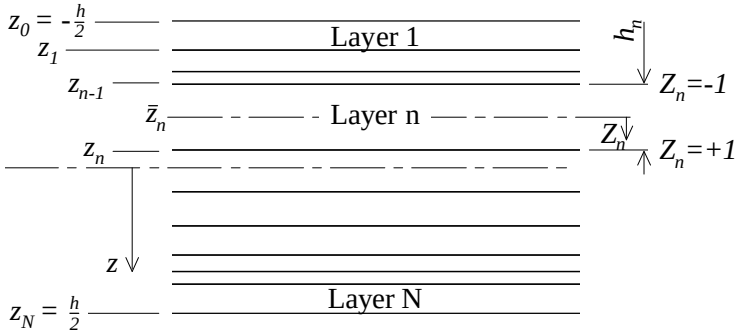

Figure 1: Laminate configuration

2.1. Stress-strain relationships

Under plane-stress conditions, the relationship between the in-plane stresses and strains in an orthotropic material can be expressed in the principal material coordinate system as

$$\boldsymbol{\sigma}^{12} = \boldsymbol{Q}\boldsymbol{\epsilon}^{12} \tag{2}$$

where $\boldsymbol{\sigma}^{12}$ and $\boldsymbol{\epsilon}^{12}$ are, respectively, matrices representing the stresses and strains and $\boldsymbol{Q}$ is the reduced stiffness matrix [60, 61]. In the above, and in the

sequel, boldface symbols represent matrices of dimension either 3×3 or 3×1. Eq. (2) can be written explicitly as

$$\begin{bmatrix} \sigma_1 \\ \sigma_2 \\ \tau_{12} \end{bmatrix} = \begin{bmatrix} Q_{11} & Q_{12} & 0 \\ Q_{12} & Q_{22} & 0 \\ 0 & 0 & Q_{66} \end{bmatrix} \begin{bmatrix} \epsilon_1 \\ \epsilon_2 \\ \gamma_{12} \end{bmatrix} \tag{3}$$

where σ_1, σ_2, and τ_{12} represent the normal stresses in the 1 and 2 directions and the shear stress in the 1-2 plane respectively. ϵ_1, ϵ_2 and γ_{12} represent the corresponding strains.

For a FGP with elastic properties varying as a function of the thickness coordinate z, it is clear that $\boldsymbol{Q}$ also varies in this direction.

When the stress strain relationship of Eq. 3 is transformed into the global coordinate system, it is assumed that the principal material coordinate system is rotated counter-clockwise relative to the global coordinate system. The stress-strain relationship in the global coordinate system is written as follows:

$$\boldsymbol{\sigma} = \bar{\boldsymbol{Q}}\boldsymbol{\epsilon} \tag{4}$$

where $\boldsymbol{\sigma}$ and $\boldsymbol{\epsilon}$ are respectively matrices representing the stresses and mechanical strains and $\bar{\boldsymbol{Q}}$ is the transformed reduced stiffness matrix. Eq. (4) can be written explicitly as

$$\begin{bmatrix} \sigma_x \\ \sigma_y \\ \tau_{xy} \end{bmatrix} = \begin{bmatrix} \bar{Q}_{11} & \bar{Q}_{12} & \bar{Q}_{16} \\ \bar{Q}_{12} & \bar{Q}_{22} & \bar{Q}_{26} \\ \bar{Q}_{16} & \bar{Q}_{26} & \bar{Q}_{66} \end{bmatrix} \begin{bmatrix} \epsilon_x \\ \epsilon_y \\ \gamma_{xy} \end{bmatrix} \tag{5}$$

where σ_x, σ_y, and τ_{xy} represent the normal stresses in the x and y directions and the shear stress in the xy plane respectively; ϵ_x, ϵ_y and γ_{xy} represent the corresponding mechanical strains.

The terms within the $\boldsymbol{Q}$ matrix of a FGP vary as a function of z. Additionally, although the authors are not aware of any material where this currently

occurs, it is potentially possible for the rotation angle of the principal material coordinate system also to vary as a function of z. The variation of individual elements of $\bar{\boldsymbol{Q}}$ with respect to the z-coordinate can consequently be very complex.

2.2. Mechanical loading

Following the usual convention, the force resultants, $\boldsymbol{N}$, can be found by integrating the in-plane stresses through the thickness of the laminate.

$$\boldsymbol{N} = \int_{-\frac{h}{2}}^{\frac{h}{2}} \boldsymbol{\sigma} \, dz \tag{6}$$

By substituting Eq. (4) into Eq. (6), and since the strain varies linearly through the thickness, Eq. (6) can be rewritten as

$$\boldsymbol{N} = \int_{-\frac{h}{2}}^{\frac{h}{2}} \bar{\boldsymbol{Q}}(\boldsymbol{\epsilon}^0 + z\boldsymbol{\kappa}) \, dz \tag{7}$$

where $\boldsymbol{\epsilon}^0$ and $\boldsymbol{\kappa}$ are the mid-plane strains and the curvatures respectively, measured relative to the global coordinate system.

The material properties are discontinuous from layer to layer. Therefore $\boldsymbol{N}$ must be found by summing the individual contributions of each layer:

$$\boldsymbol{N} = \sum_{n=1}^{N} \int_{z_{n-1}}^{z_n} \bar{\boldsymbol{Q}}_n(\boldsymbol{\epsilon}^0 + z\boldsymbol{\kappa}) \, dz \tag{8}$$

where $\bar{\boldsymbol{Q}}_n$ is the transformed stiffness matrix of layer n.

At this stage it becomes apparent that, unless the z-variation of the terms within $\bar{\boldsymbol{Q}}_n$ are represented by simple functions, the explicit integration of Eq. (8) is impossible. Accordingly each of the terms in $\bar{\boldsymbol{Q}}_n$ is represented by a polynomial series in Z_n through curve fitting. If sufficiently high order terms are used in the polynomial, the fitted curve can accurately represent the original function.

Since a polynomial series of order P is fitted to each term within $\bar{\boldsymbol{Q}}_n$, it can be written as

$$\bar{\boldsymbol{Q}}_n = \sum_{p=0}^{P} \begin{bmatrix} \bar{Q}_{11_{n_p}} & \bar{Q}_{12_{n_p}} & \bar{Q}_{16_{n_p}} \\ \bar{Q}_{12_{n_p}} & \bar{Q}_{22_{n_p}} & \bar{Q}_{26_{n_p}} \\ \bar{Q}_{16_{n_p}} & \bar{Q}_{26_{n_p}} & \bar{Q}_{66_{n_p}} \end{bmatrix} Z_n^p \tag{9}$$

where the matrix on the right hand side of the equation represents the coefficients of the p^{th} terms in the series used to describe $\bar{\boldsymbol{Q}}_n$.

Let $\bar{\boldsymbol{Q}}_{n_p}$ denote the p^{th} matrix on the right hand side of Eq. (9).

$$\bar{\boldsymbol{Q}}_{n_p} = \begin{bmatrix} \bar{Q}_{11_{n_p}} & \bar{Q}_{12_{n_p}} & \bar{Q}_{16_{n_p}} \\ \bar{Q}_{12_{n_p}} & \bar{Q}_{22_{n_p}} & \bar{Q}_{26_{n_p}} \\ \bar{Q}_{16_{n_p}} & \bar{Q}_{26_{n_p}} & \bar{Q}_{66_{n_p}} \end{bmatrix} \tag{10}$$

Eq. (9) can now be rewritten in a more concise form:

$$\bar{\boldsymbol{Q}}_n = \sum_{p=0}^{P} \bar{\boldsymbol{Q}}_{n_p}\ Z_n^p \tag{11}$$

By substituting Eq. (11) into Eq. (8) and changing the variable of integration within each layer to Z_n, the integral terms in Eq. (8) are readily evaluated.

$$\begin{aligned} \boldsymbol{N} &= \sum_{n=1}^{N} \int_{-1}^{1} \sum_{p=0}^{P} \bar{\boldsymbol{Q}}_{n_p} Z_n^{\,p} \left(\boldsymbol{\epsilon}^0 + (\bar{z}_n + \frac{h_n}{2} Z_n)\boldsymbol{\kappa} \right) \frac{h_n}{2}\ dZ_n \\ &= \sum_{n=1}^{N} \frac{h_n}{2} \sum_{p=0}^{P} \bar{\boldsymbol{Q}}_{n_p} \int_{-1}^{1} \left(Z_n^p \boldsymbol{\epsilon}^0 + (\bar{z}_n Z_n^p + \frac{h_n}{2} Z_n^{p+1})\boldsymbol{\kappa} \right)\ dZ_n \\ &= \sum_{n=1}^{N} \frac{h_n}{2} \left(\sum_{p=0,2,4\ldots}^{P} \frac{2}{p+1} \bar{\boldsymbol{Q}}_{n_p} \right) \boldsymbol{\epsilon}^0 \\ &\quad + \sum_{n=1}^{N} \frac{h_n}{2} \left(\sum_{p=0,2,4\ldots}^{P} \frac{2\bar{z}_n}{p+1} \bar{\boldsymbol{Q}}_{n_p} + \sum_{p=1,3,5\ldots}^{P} \frac{h_n}{p+2} \bar{\boldsymbol{Q}}_{n_p} \right) \boldsymbol{\kappa} \end{aligned} \tag{12}$$

Likewise the moment resultants, $\boldsymbol{M}$, can be determined as follows:

$$
\begin{aligned}
\boldsymbol{M} &= \sum_{n=1}^{N} \int_{z_{n-1}}^{z_n} \bar{\boldsymbol{Q}}_n(\boldsymbol{\epsilon}^0 + z\boldsymbol{\kappa}) z \, dz \\
&= \sum_{n=1}^{N} \frac{h_n}{2} \left[\sum_{p=0,2,4\ldots}^{P} \frac{2\bar{z}_n}{p+1} \bar{\boldsymbol{Q}}_{n_p} + \sum_{p=1,3,5\ldots}^{P} \frac{h_n}{p+2} \bar{\boldsymbol{Q}}_{n_p} \right] \boldsymbol{\epsilon}^0 \\
&\quad + \sum_{n=1}^{N} \frac{h_n}{2} \left[\sum_{p=0,2,4\ldots}^{P} \left(\frac{2\bar{z}_n^2}{p+1} + \frac{h_n^2}{2(p+3)} \right) \bar{\boldsymbol{Q}}_{n_p} \right. \\
&\quad \left. + \sum_{p=1,3,5\ldots}^{P} \frac{2\bar{z}_n h_n}{p+2} \bar{\boldsymbol{Q}}_{n_p} \right] \boldsymbol{\kappa}
\end{aligned}
\tag{13}
$$

If the force and moment resultants are related to the mid-plane strains and curvatures in the usual manner [60, 61]

$$
\begin{bmatrix} \boldsymbol{N} \\ \boldsymbol{M} \end{bmatrix} = \begin{bmatrix} \boldsymbol{A} & \boldsymbol{B} \\ \boldsymbol{B} & \boldsymbol{D} \end{bmatrix} \begin{bmatrix} \boldsymbol{\epsilon}^0 \\ \boldsymbol{\kappa} \end{bmatrix}
\tag{14}
$$

then the terms $\boldsymbol{A}$, $\boldsymbol{B}$ and $\boldsymbol{D}$ can be found as

$$
\boldsymbol{A} = \sum_{n=1}^{N} h_n \sum_{p=0,2,4\ldots}^{P} \frac{1}{p+1} \bar{\boldsymbol{Q}}_{n_p}
\tag{15}
$$

$$
\boldsymbol{B} = \sum_{n=1}^{N} h_n^2 \left[\sum_{p=0,2,4\ldots}^{P} \frac{(\bar{z}_n/h_n)}{p+1} \bar{\boldsymbol{Q}}_{n_p} + \sum_{p=1,3,5\ldots}^{P} \frac{1}{2(p+2)} \bar{\boldsymbol{Q}}_{n_p} \right]
\tag{16}
$$

$$
\begin{aligned}
\boldsymbol{D} = \sum_{n=1}^{N} h_n^3 \left[\sum_{p=0,2,4\ldots}^{P} \left(\frac{(\bar{z}_n/h_n)^2}{p+1} + \frac{1}{4(p+3)} \right) \bar{\boldsymbol{Q}}_{n_p} \right. \\
\left. + \sum_{p=1,3,5\ldots}^{P} \frac{(\bar{z}_n/h_n)}{p+2} \bar{\boldsymbol{Q}}_{n_p} \right]
\end{aligned}
\tag{17}
$$

It is worth noting a few special characteristics of these matrices. The odd terms of p do not contribute to $\boldsymbol{A}$. Since the odd terms are antisymmetrical about $\bar{z}_n$, this is expected. For instance, an increase in stiffness on one side of $\bar{z}_n$ is exactly counteracted by a reduction in stiffness on the opposite side.

Unlike $\boldsymbol{A}$, both $\boldsymbol{B}$ and $\boldsymbol{D}$ are required to contain both odd and even terms since the position of each layer within the laminate contributes to the coupling and flexural stiffness matrices respectively. The effects of antisymmetrical terms in each layer cannot therefore be cancelled in the same way as occurs for the extensional stiffness matrix, $\boldsymbol{A}$.

When the laminate is symmetrical, $\boldsymbol{B}$ is required to be zero. By considering the first series within Eq. (16), which contains symmetrical terms (even values of p), it is apparent that for a symmetrical laminate there is a value of exactly $-\bar{z}_n$ for every value of $\bar{z}_n$ and so this series has zero value. Likewise for the second series, containing antisymmetrical terms (odd values of p), symmetry requires that for every layer with a particular stiffness variation, another layer exists with an exactly opposite variation. This means that every $\bar{\boldsymbol{Q}}_{n_p}$ in the series with odd terms is cancelled by a term $-\bar{\boldsymbol{Q}}_{n_p}$ in the symmetrically opposite layer and so $\boldsymbol{B}$ is indeed zero for symmetrical laminates.

2.3. Hygrothermal loading

The unconstrained thermal strains of an orthotropic material in the global coordinate system can be found as

$$\boldsymbol{\epsilon}_T = \boldsymbol{\alpha}\Delta T \tag{18}$$

where the subscript T refers to thermal loading, $\boldsymbol{\alpha}$ is a matrix of coefficients of thermal expansion, and ΔT is the change in temperature.

The terms of $\boldsymbol{\alpha}$ can show substantial variation in the $z-$direction. This is because the coefficients of thermal expansion in a FGM as measured in the principal material coordinate system, and potentially also the angle of rotation of this coordinate system relative to the global coordinate system, can vary

through the thickness. For the same reasons that polynomial series are fitted to the terms of $\bar{\boldsymbol{Q}}_n$, it is elected to fit polynomial series to each of the terms of $\boldsymbol{\alpha}$ for every layer n.

The through-thickness variation in $\boldsymbol{\alpha}$ for layer n can thus be expressed as

$$\boldsymbol{\alpha}_n = \sum_{q=0}^{Q} \boldsymbol{\alpha}_{n_q} Z_n^q \tag{19}$$

where $\boldsymbol{\alpha}_{n_q}$ represents the coefficients of the q^{th} term in the series used to describe $\boldsymbol{\alpha}_n$.

Likewise the temperature can vary through the thickness and so the actual temperature variation within layer n is expressed as a polynomial series:

$$\Delta T_n = \sum_{r=0}^{R} T_{n_r} Z_n^r \tag{20}$$

where T_{n_r} represents the coefficients of the r^{th} term in the series used to describe ΔT_n.

The thermal force and moment resultants, N_T and M_T respectively, can thus be determined in the same way as they are found for mechanical loading:

$$\begin{aligned}
\boldsymbol{N}_T &= \int_{-\frac{h}{2}}^{\frac{h}{2}} \boldsymbol{\sigma}_T \, dz \\
&= \sum_{n=1}^{N} \int_{z_{n-1}}^{z_n} \bar{\boldsymbol{Q}}_n \boldsymbol{\epsilon}_{nT} \, dz \\
&= \sum_{n=1}^{N} \frac{h_n}{2} \int_{-1}^{1} \sum_{p=0}^{P} \bar{\boldsymbol{Q}}_{n_p} Z_n^p \left(\sum_{q=0}^{Q} \boldsymbol{\alpha}_{n_q} Z_n^q \sum_{r=0}^{R} T_{n_r} Z_n^r \right) dZ_n \\
&= \sum_{n=1}^{N} \frac{h_n}{2} \sum_{p=0}^{P} \sum_{q=0}^{Q} \sum_{r=0}^{R} \bar{\boldsymbol{Q}}_{n_p} \boldsymbol{\alpha}_{n_q} T_{n_r} \left(\frac{1-(-1)^{p+q+r+1}}{p+q+r+1} \right)
\end{aligned} \tag{21}$$

and

$$\boldsymbol{M}_T = \sum_{n=1}^{N} \frac{h_n}{2} \sum_{p=0}^{P} \sum_{q=0}^{Q} \sum_{r=0}^{R} \bar{\boldsymbol{Q}}_{n_p} \boldsymbol{\alpha}_{n_q} T_{n_r} \left(\bar{z}_n \frac{1-(-1)^{p+q+r+1}}{p+q+r+1} + \frac{h_n}{2} \frac{1-(-1)^{p+q+r+2}}{p+q+r+2} \right) \tag{22}$$

The effects of moisture absorption are analogous to those of temperature changes. In the global coordinate system, the unconstrained strains due to moisture absorption can be given as

$$\boldsymbol{\epsilon}_H = \boldsymbol{\beta} \Delta H \tag{23}$$

where the subscript H refers to the effects of moisture absorption, $\boldsymbol{\beta}$ is a matrix of coefficients of hygroscopic expansion, and ΔH is the change in moisture content. The term $\boldsymbol{\beta}$ is defined analogously to $\boldsymbol{\alpha}$ and so the through-thickness variation in $\boldsymbol{\beta}$ within layer n is also expressed in polynomial form as

$$\boldsymbol{\beta}_n = \sum_{f=0}^{F} \boldsymbol{\beta}_{n_f} Z_n^f \tag{24}$$

Like the temperature, the moisture content can also vary through the thickness. The variation in moisture content within layer n is expressed as

$$\Delta H_n = \sum_{g=0}^{G} H_{n_g} Z_n^g \tag{25}$$

where H_{n_g} represents the coefficients of the g^{th} term in the series used to describe ΔH_n.

Since the effects of moisture absorption are analogous to those of changes in temperature, the expressions for the force and moment resultants, N_H and M_H, are similar to those of N_T and M_T:

$$\boldsymbol{N}_H = \sum_{n=1}^{N} \frac{h_n}{2} \sum_{p=0}^{P} \sum_{f=0}^{F} \sum_{g=0}^{G} \bar{\boldsymbol{Q}}_{n_p} \boldsymbol{\beta}_{n_f} H_{n_g} \left(\frac{1-(-1)^{p+f+g+1}}{p+f+g+1} \right) \tag{26}$$

$$\boldsymbol{M}_H = \sum_{n=1}^{N} \frac{h_n}{2} \sum_{p=0}^{P} \sum_{f=0}^{F} \sum_{g=0}^{G} \bar{\boldsymbol{Q}}_{n_p} \boldsymbol{\beta}_{n_f} H_{n_g} \left(\bar{z}_n \frac{1-(-1)^{p+f+g+1}}{p+f+g+1} + \frac{h_n}{2} \frac{1-(-1)^{p+f+g+2}}{p+f+g+2} \right) \tag{27}$$

The force and moment resultants arising from hygrothermal loading combine with those from mechanical loading to produce deformations in the laminate. Eq. (14) can thus be updated to reflect the contribution of hygrothermal loads:

$$\begin{bmatrix} \boldsymbol{N} + \boldsymbol{N}_T + \boldsymbol{N}_H \\ \boldsymbol{M} + \boldsymbol{M}_T + \boldsymbol{M}_H \end{bmatrix} = \begin{bmatrix} \boldsymbol{A} & \boldsymbol{B} \\ \boldsymbol{B} & \boldsymbol{D} \end{bmatrix} \begin{bmatrix} \boldsymbol{\epsilon}^0 \\ \boldsymbol{\kappa} \end{bmatrix} \tag{28}$$

2.4. Piezoelectric loading

Loading of piezoelectric materials in actuator mode is handled in the same manner as hygrothermal loading. The strains in the principal material coordinate system of a piezoceramic poled in the thickness (or 3-) direction and subjected to an electric field, $V^{'}$, aligned in the same direction can be expressed as [62, 63]

$$\begin{bmatrix} \epsilon_1 \\ \epsilon_2 \\ \gamma_{12} \end{bmatrix} = \begin{bmatrix} d_{31} \\ d_{32} \\ 0 \end{bmatrix} V^{'} \tag{29}$$

where d_{31} and d_{32} are piezoelectric strain constants.

When transformed into the global coordinate system, this relationship can be written as

$$\boldsymbol{\epsilon}_{V^{'}} = \boldsymbol{d} V^{'} \tag{30}$$

where $\boldsymbol{d}$ is defined as

$$\boldsymbol{d} = \begin{bmatrix} d_{zx} \\ d_{zy} \\ d_{zxy} \end{bmatrix} = \begin{bmatrix} d_{31}\cos^2\theta + d_{32}\sin^2\theta \\ d_{31}\sin^2\theta + d_{32}\cos^2\theta \\ 2(d_{31} - d_{32})\sin\theta\cos\theta \end{bmatrix} \tag{31}$$

where θ defines the rotation angle of the material principal coordinate system relative to the global coordinate system. The terms d_{zx}, d_{zy} and d_{zxy} in Eq. (31) are piezoelectric strain constants relating ϵ_x, ϵ_y and γ_{xy} to an electric field aligned in the z-direction.

Since both the piezoelectric strain constants and the electric field strength within layer n could change in the through-thickness direction, they are written as polynomial series:

$$\boldsymbol{d}_n = \sum_{l=0}^{L} \boldsymbol{d}_{n_l} Z_n^l \tag{32}$$

$$V_n^{'} = \sum_{m=0}^{M} V_{n_m}^{'} Z_n^m \tag{33}$$

The form of the piezoelectric strains is identical to that of hygrothermal strains. The form of the force and moment resultants arising from piezoelectric loading, $\boldsymbol{N}_{V'}$ and $\boldsymbol{M}_{V'}$ respectively, is consequently identical to that of $\boldsymbol{N}_T$ and $\boldsymbol{M}_T$:

$$\boldsymbol{N}_{V'} = \sum_{n=1}^{N} \frac{h_n}{2} \sum_{p=0}^{P} \sum_{l=0}^{L} \sum_{m=0}^{M} \bar{\boldsymbol{Q}}_{n_p} \boldsymbol{d}_{n_l} V_{n_m}^{'} \left(\frac{1-(-1)^{p+l+m+1}}{p+l+m+1} \right) \tag{34}$$

$$\boldsymbol{M}_{V'} = \sum_{n=1}^{N} \frac{h_n}{2} \sum_{p=0}^{P} \sum_{l=0}^{L} \sum_{m=0}^{M} \bar{\boldsymbol{Q}}_{n_p} \boldsymbol{d}_{n_l} V_{n_m}^{'} \left(\bar{z}_n \frac{1-(-1)^{p+l+m+1}}{p+l+m+1} + \frac{h_n}{2} \frac{1-(-1)^{p+l+m+2}}{p+l+m+2} \right) \tag{35}$$

When Eq. (28) is updated to reflect the effect of piezoelectric loading, it takes the form

$$\begin{bmatrix} \boldsymbol{N} + \boldsymbol{N}_T + \boldsymbol{N}_H + \boldsymbol{N}_{V'} \\ \boldsymbol{M} + \boldsymbol{M}_T + \boldsymbol{M}_H + \boldsymbol{M}_{V'} \end{bmatrix} = \begin{bmatrix} \boldsymbol{A} & \boldsymbol{B} \\ \boldsymbol{B} & \boldsymbol{D} \end{bmatrix} \begin{bmatrix} \boldsymbol{\epsilon}^0 \\ \boldsymbol{\kappa} \end{bmatrix} \tag{36}$$

2.5. Calculation of stresses

Once $\boldsymbol{\epsilon}^0$ and $\boldsymbol{\kappa}$ are known, the mechanical strains are calculated by subtracting the hygrothermal and piezoelectric strains from the total strains. In the general case, a plate may be subjected to mechanical, hygrothermal and piezoelectric loading and so the in-plane variation of the mechanical strains is found as follows:

$$\boldsymbol{\epsilon} = \boldsymbol{\epsilon}^0 + z\boldsymbol{\kappa} - \boldsymbol{\alpha}\Delta T - \boldsymbol{\beta}\Delta H - \boldsymbol{d}V^{'} \tag{37}$$

The stresses may now be found using Eq. 4.

3. Demonstration problems

To demonstrate the use and accuracy of the method presented in the previous sections, the problem presented by Reddy and Cheng [13] is considered. These authors obtained three-dimensional solutions for a functionally graded rectangular plate, simply supported on all edges, and subjected individually to mechanical and thermal loadings. Results obtained using the present method are compared against those of Reddy and Cheng [13] for each of these loads.

The plate configuration is presented in Fig. 2.

The boundary conditions applied to the plate are as follows:

$$\begin{aligned} v = w = \sigma_x = 0, \quad \text{at } x = 0, a \\ u = w = \sigma_y = 0, \quad \text{at } y = 0, b \end{aligned} \tag{38}$$

The plate material progressively changes from pure Monel (70Ni-30Cu) at $z = \frac{-h}{2}$ to pure zirconia at $z = \frac{h}{2}$. The properties of these materials are listed in Table 1.

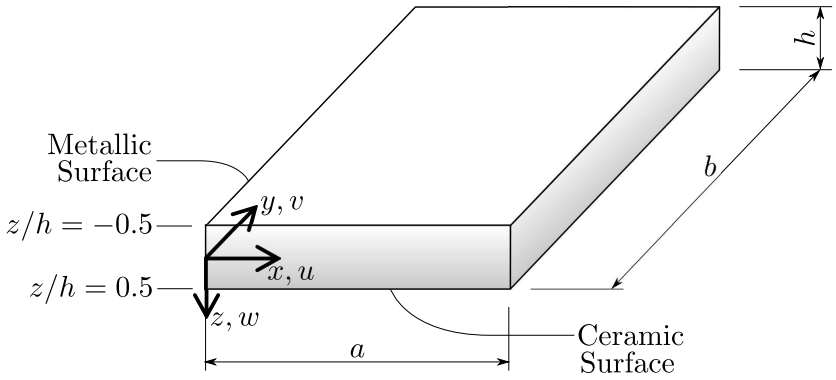

Figure 2: Configuration of functionally graded plate under consideration

Table 1: Material properies of plate constituents [13]

	Monel	Zirconia
Bulk modulus, K (GPa)	227.24	125.83
Shear modulus, μ (GPa)	65.55	58.077
Coefficient of thermal expansion, α $(/K)$	15×10^{-6}	10×10^{-6}
Heat conductivity coefficient, κ (W/mK)	25	2.09

The volume fraction of the ceramic phase, V_c, varies according to a power law:

$$V_c = (\frac{1}{2} + \frac{z}{h})^{\lambda} \tag{39}$$

where λ is a constant that dictates the variation in the profile of the material properties. Reddy and Cheng considered three different values of λ: $\frac{1}{2}$, 1 and 2. These values are used in the present work to allow the comparison of results.

The locally effective material properties within the plate are calculated using Eqs. 40 through 43 provided by Reddy and Cheng [13]. In these equations the subscripts m and c refer to the metallic and ceramic phases respectively.

$$\frac{K - K_m}{K_c - K_m} = \frac{V_c}{1 + (1 - V_c)\dfrac{K_c - K_m}{K_m + \dfrac{4}{3}\mu_m}} \tag{40}$$

$$\frac{\mu - \mu_m}{\mu_c - \mu_m} = \frac{V_c}{1 + (1 - V_c)\dfrac{\mu_c - \mu_m}{\mu_m + f_m}} \tag{41}$$

where

$$f_m = \frac{\mu_m(9K_m + 8\mu_m)}{6(K_m + 2\mu_m)}$$

$$\frac{\alpha - \alpha_m}{\alpha_c - \alpha_m} = \frac{\dfrac{1}{K} - \dfrac{1}{K_m}}{\dfrac{1}{K_c} - \dfrac{1}{K_m}} \tag{42}$$

$$\frac{\kappa - \kappa_m}{\kappa_c - \kappa_m} = \frac{V_c}{1 + (1 - V_c)\dfrac{\kappa_c - \kappa_m}{3\kappa_m}} \tag{43}$$

3.1. Mechanical loading

The first of the two load cases considered arises from mechanical loading. Pressure, q, is applied to the ceramic surface of the plate according to the following equation:

$$q = q_0 \sin(\frac{x}{a}\pi) \sin(\frac{y}{b}\pi) \tag{44}$$

where q_0 represents the pressure at the centre of the plate.

The pressure distribution on the plate is presented in Fig. 3.

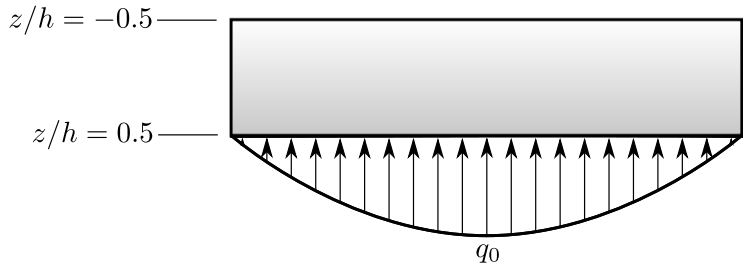

Figure 3: Pressure distribution applied to plate

3.1.1. Solution

The present technique requires that the variation in material properties be represented by polynomial series. The through-thickness variation of each term in the $\bar{\boldsymbol{Q}}$ matrix of Eq. 4 is consequently determined and a polynomial series fitted. For $\lambda = 1$ and $\lambda = 2$ it is found that a 6^{th} order polynomial series is accurate to four significant figures. The variation in material properties corresponding to $\lambda = \frac{1}{2}$ requires a much higher order polynomial series. In fact, a 25^{th} order series is used. The $\boldsymbol{A}$, $\boldsymbol{B}$ and $\boldsymbol{D}$ matrices are calculated using Eqs. 15 through 17.

The material properties are not symmetric through the thickness of the plate and so coupling between bending and extension occurs. The problem is solved through the use of the Rayleigh-Ritz technique. The following displacement functions are assumed since they identically satisfy the geometric boundary conditions:

$$u = \sum_{m=1}^{M}\sum_{n=1}^{N} U_{mn}\, \cos\left(m\pi\frac{x}{a}\right)\, \sin\left(n\pi\frac{y}{b}\right) \tag{45a}$$

$$v = \sum_{p=1}^{P}\sum_{q=1}^{Q} V_{pq}\, \sin\left(p\pi\frac{x}{a}\right)\, \cos\left(q\pi\frac{y}{b}\right) \tag{45b}$$

$$w = \sum_{r=1}^{R}\sum_{s=1}^{S} W_{rs}\, \sin\left(r\pi\frac{x}{a}\right)\, \sin\left(s\pi\frac{y}{b}\right) \tag{45c}$$

where U_{mn}, V_{pq} and W_{rs} are displacement coefficients.

Since the applied loading, q, is sinusoidal with only a single half-wave in both the x and y directions, the displacement functions of Eq. 45 each degenerate to a single term with $M = N = P = Q = R = S = 1$. The midplane strains and curvatures of the plate, $\boldsymbol{\epsilon}^0$ and $\boldsymbol{\kappa}$ respectively, are found from the appropriate differential functions of Eq. 45. Stresses are then determined as described in section 2.5. The through-thickness variation of in-plane displacement is determined by adding the contribution of slope, arising from curvature of the plate, to the in-plane displacements determined using Eqs. 45a and 45b. The through-thickness variation in out-of-plane displacement is calculated by integrating the Poisson's strains from the mid-plane outwards and adding the resulting out-of-plane displacement variation to the displacement of the mid-plane found using Eq. 45c.

3.1.2. Results and discussion

The peak out-of-plane displacement occurs at the centre of the plate whereas the peak in-plane displacements occur at the midpoint of the plate edges. The peak displacement in the x direction occurs at $y = 0$ and that in the y direction occurs at $x = 0$. For a square plate, the peak in-plane displacements are the same in both the x and y directions. The non-dimensionalized form of the peak displacements is given by

$$\bar{u} = \frac{u(z)}{\frac{q_0}{K^*}a} \tag{46}$$

and

$$\bar{w} = \frac{w(z)}{\frac{q_0}{K^*}a} \tag{47}$$

where $K^* = 1$ GPa.

The peak in-plane stress, which occurs at the centre of the plate, is non-

dimensionalized as

$$\bar{\sigma}_x = \frac{\sigma_x(z)}{q_0} \tag{48}$$

Figs. 4 through 6 provide a comparison of results obtained using the present method against the published results of Reddy and Cheng [13]. Out-of-plane stresses cannot be directly calculated using the present method and so they are not given.

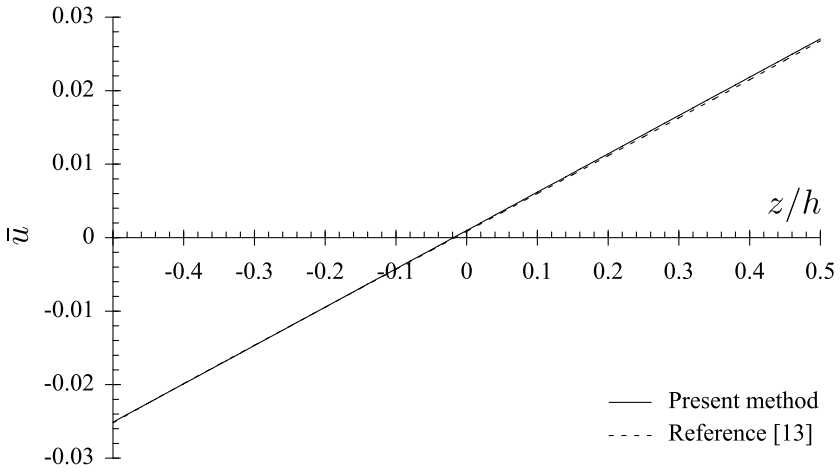

Figure 4: Through-thickness variation of normalized in-plane deflection ($a/h = 10,\ \lambda = 1$)

It is apparent from Figs. 4 and 5 that the through-thickness variation of the in-plane deflections and stresses predicted by the present method are almost indistinguishable from those predicted by a full three-dimensional analysis. Although Fig. 6 shows that the out-of-plane deflection is less accurately predicted, the error in the results is only about 4%. Since the present method neglects the effect of through-thickness shear strains, the predicted deflection is smaller than that of Reddy and Cheng [13].

Table 2 provides a comparison of $\bar{u}$, $\bar{w}$ and $\bar{\sigma}_x$ for plate aspect ratios of 50 and 10 with $\lambda = 2$. The listed error values correspond to those at the maximum displacement or stress for each aspect ratio.

It is evident from Table 2 that the results obtained by the present method are in excellent agreement with those of Reddy and Cheng [13] at an aspect ratio of

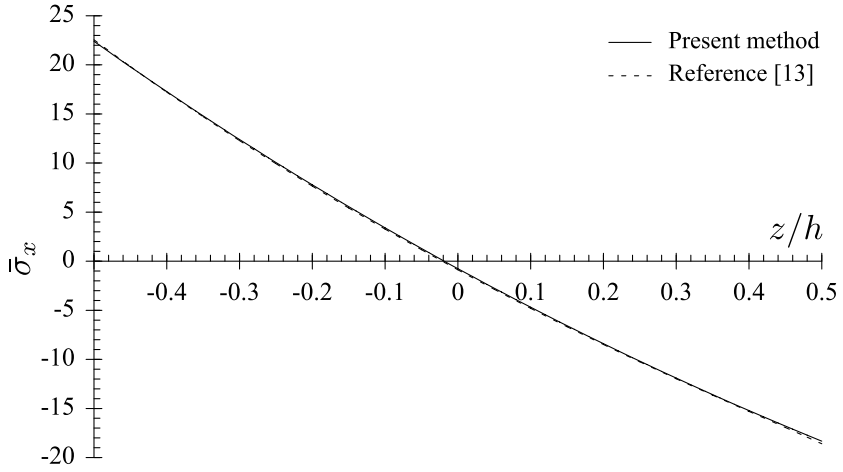

Figure 5: Through-thickness variation of normalized in-plane stress ($a/h = 10,\ \lambda = 1$)

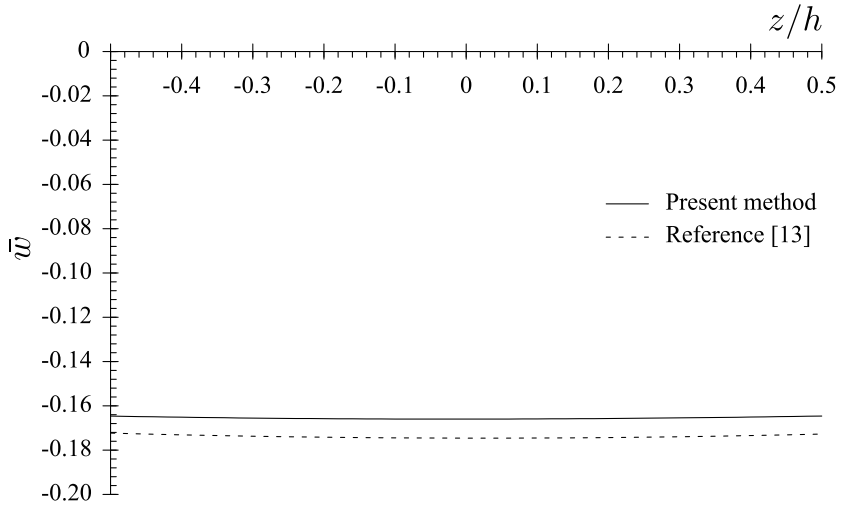

Figure 6: Through-thickness variation of normalized out-of-plane deflection ($a/h = 10,\ \lambda = 1$)

Table 2: Comparison of displacements and stresses for a square plate under mechanical load, $\lambda = 2$

	$a/h = 50$		$a/h = 10$	
	3D	Present	3D	Present
$\bar{u}$ $(\frac{-h}{2})$	-0.6141	-0.6139	-0.02472	-0.02456
$\bar{u}$ (0)	0.02312	0.02335	0.0007108	0.0009339
$\bar{u}$ $(\frac{h}{2})$	0.6603	0.6606	0.02617	.02642
Error		0.0454%		0.955%
$\bar{\sigma}_x$ $(\frac{-h}{2})$	548.0	547.8	22.06	21.91
$\bar{\sigma}_x$ (0)	-19.56	-19.47	-0.8722	–0.7788
$\bar{\sigma}_x$ $(\frac{h}{2})$	-447.9	-447.7	-18.17	-17.91
Error		-0.0365%		-0.680%
$\bar{w}$ $(\frac{-h}{2})$	-20.32	-20.28	-0.1685	-0.1609
$\bar{w}$ (0)	-20.33	-20.28	-0.1707	-0.1623
$\bar{w}$ $(\frac{h}{2})$	-20.32	-20.28	-0.1689	-0.1609
Error		-0.246%		-4.92%

3D results extracted from Reddy and Cheng [13].

50. At an aspect ratio of 10, the magnitude of the errors increases slightly. The in-plane deflection and stress results are, however, still accurate to within 1% and the out-of plane deflection is accurate to within 5%. The increasing error with decreasing aspect ratio is expected as the thick plate regime is approached.

3.2. Thermal loading

The second load case considered by Reddy and Cheng [13] corresponds to that of thermal loading. A temperature distribution is applied to the ceramic surface of the plate according to

$$T = T_0 \sin(\frac{x}{a}\pi) \sin(\frac{y}{b}\pi) \tag{49}$$

where T_0 represents the temperature at the centre of the plate.

The temperature on all other surfaces is maintained constant. The temperature distribution applied to the plate is illustrated in Fig. 7.

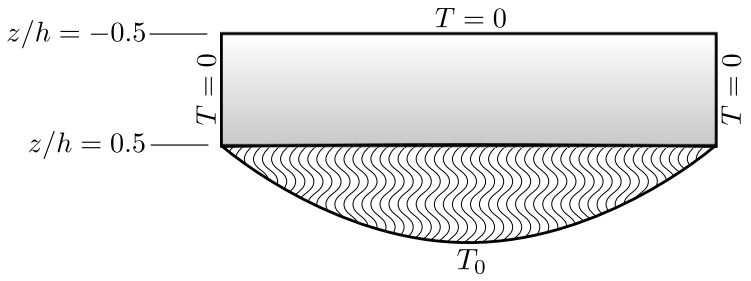

Figure 7: Temperature distribution applied to plate

3.2.1. Solution

Before the displacements and stresses in the plate are determined, it is necessary to find the through-thickness temperature distribution. This is affected by heat flow into the sides of the plate and is calculated using the method described by Brischetto *et al.* [46]. The plate is discretized into a number of layers. Each layer is assumed to have uniform thermal properties through its thickness. The temperature distribution is calculated subject to the requirement that heat is allowed to flow out of the edges of each layer to satisfy the boundary conditions and the temperatures and heat flows are identical in the mating surfaces of adjacent layers. One hundred layers were used in the present work.

The resulting non-dimensional temperature distributions are illustrated in Fig. 8 where $\bar{T} = \frac{T(z)}{T_0}$. The calculated temperature distributions are indistinguishable from those presented by Reddy and Cheng [13].

The $\boldsymbol{A}$, $\boldsymbol{B}$ and $\boldsymbol{D}$ matrices are calculated using the same approach employed for the problem of mechanical loading. Once the through thickness temperature distribution is known, it is represented by a 15^{th} order polynomial series which is accurate to four significant figures. The thermal loading at the centre of the plate is then calculated using Eqs. 21 and 22. Since the temperature distribution remains sinusoidal at all z locations [46], the thermal loading is also sinusoidally distributed.

The problem is solved using the Rayleigh-Ritz technique in the same manner as for the transverse pressure problem. Since the applied thermal loads are

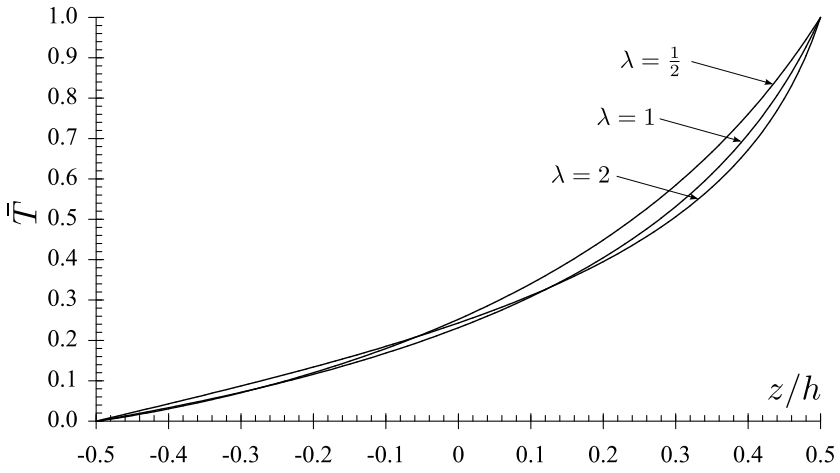

Figure 8: Through-thickness variation of normalized temperature

sinusoidal with a only single half-wave in both the x and y directions, the displacement functions of Eq. 45 degenerate to the first term.

The through-thickness variations of in-plane displacement and stress are found in the same way as for mechanical loading. The variation in out-of-plane displacement is found by adding the through-thickness displacements arising from thermal strains and those due to Poisson's strains to the displacement of the mid-plane.

3.2.2. Results and discussion

The peak in- and out-of-plane displacements occur at the same locations as for mechanical loading. These displacements are, however, non-dimensionalized differently for this loading case:

$$\bar{u} = \frac{u(z)}{a\alpha^* T_0} \tag{50}$$

$$\bar{w} = \frac{w(z)}{a\alpha^* T_0} \tag{51}$$

where $\alpha^* = 10^{-6}/K$ GPa.

The peak in-plane stress is also non-dimensionalized differently to that obtained in the case of mechanical loading. The non-dimensional stress is found as

$$\bar{\sigma}_x = \frac{\sigma_x(z)}{K^* \alpha^* T_0} \tag{52}$$

where $K^* = 1$ GPa.

Graphical representations of the variation in $\bar{u}$, $\bar{w}$ and $\bar{\sigma}_x$ with z are provided by Reddy and Cheng [13] for plates with an aspect ratio of 10 and λ equal to $\frac{1}{2}$, 1 and 2. Results obtained using the present method are compared against the published results in Figs. 9 through 11. As for the case of mechanical loading, it is not possible to directly calculate the out-of-plane stresses using the present method and so they are not shown.

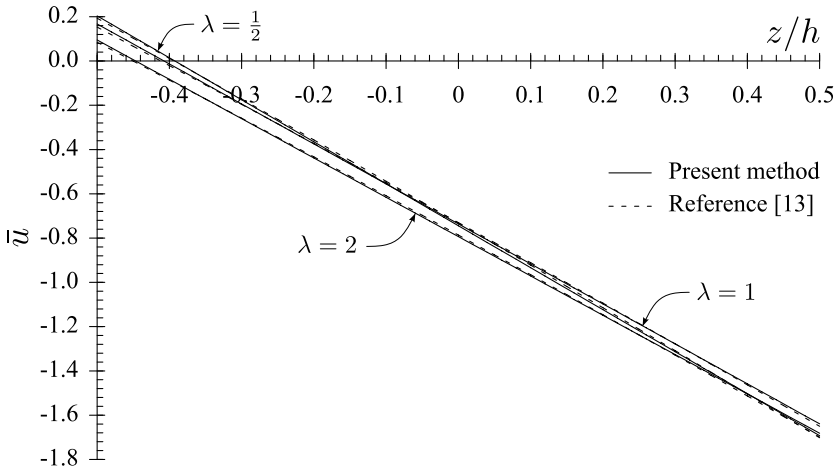

Figure 9: Through-thickness variation of normalized in-plane deflection ($a/h = 10$)

Figures 9 through 11 show that the variation in displacement and stress predictions obtained by the present method are almost indistinguishable from those obtained using the full three-dimensional solution of Reddy and Cheng [13]. Unlike the case of mechanical loading, the out-of-plane displacement is accurately predicted in the case of thermal loading. The improvement can be attributed to the lack of a directly applied shear load in the latter case.

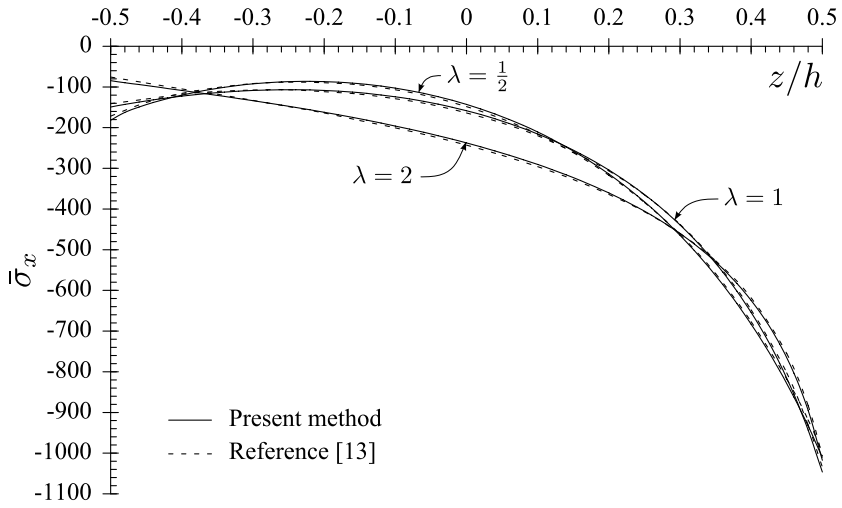

Figure 10: Through-thickness variation of normalized in-plane stress ($a/h = 10$)

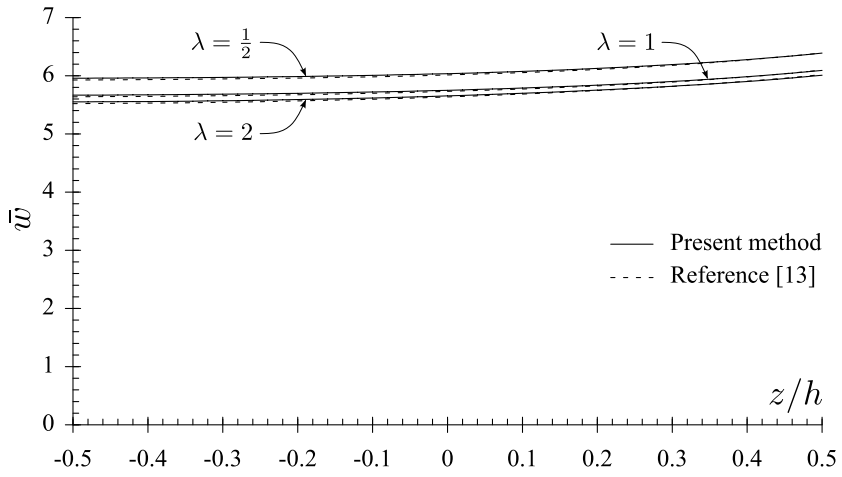

Figure 11: Through-thickness variation of normalized out-of-plane deflection ($a/h = 10$)

Further comparison of results obtained using the present method is possible using quantitative data on the variation of $\bar{u}$, $\bar{w}$ and $\bar{\sigma}_x$ with plate aspect ratio listed in the work of Reddy and Cheng [13]. This comparison is presented in Table 3 for aspect ratios of 50 and 10 for a plate with $\lambda = 2$. The errors listed in this table correspond to those at the maximum displacement or stress for each aspect ratio.

Table 3: Comparison of displacements and stresses for a square plate under thermal load, $\lambda = 2$

	$a/h = 50$		$a/h = 10$	
	3D	Present	3D	Present
$\bar{u}$ $(\frac{-h}{2})$	0.08528	0.08570	0.08492	0.09485
$\bar{u}$ (0)	-0.8081	-0.8082	-0.7862	-0.7933
$\bar{u}$ $(\frac{h}{2})$	-1.703	-1.702	-1.699	-1.681
Error		-0.0587%		-1.06%
$\bar{\sigma}_x$ $(\frac{-h}{2})$	-76.10	-76.44	-75.78	-84.61
$\bar{\sigma}_x$ (0)	-251.2	-251.0	-243.0	-237.5
$\bar{\sigma}_x$ $(\frac{h}{2})$	-1003	-1004	-1006	-1018
Error		0.0997%		1.19%
$\bar{w}$ $(\frac{-h}{2})$	28.43	28.43	5.522	5.552
$\bar{w}$ (0)	28.45	28.45	5.635	5.654
$\bar{w}$ $(\frac{h}{2})$	28.53	28.53	6.021	6.009
Error		0.000%		-0.199%

3D extracted from Reddy and Cheng [13].

As in the case of mechanical loading, it can be seen from Table 3 that the present method provides results that are in excellent agreement with those of the full three-dimensional solution at an aspect ratio of 50. The errors in this case are all below 0.1%. These errors are expected to increase as the aspect ratio decreases towards those of thick plates. At an aspect ratio of 10, the errors are slightly higher than those at an aspect ratio of 50 but the in-plane stress and displacements are still accurate to approximately 1%. The out-of-plane deflection is accurate to within 0.2%.

3.2.3. Comparison with CLT

The thermal problem is also solved using CLT so that the results can be compared with those of the present method. The plate is discretized into a number of layers and the material properties and temperature at the mid-plane of each layer are taken as constant across the full thickness of that layer.

To compare the in-plane stresses calculated using the two approaches, the through-thickness variation in $\bar{\sigma}_x$ is plotted in Fig. 12 for a plate of $\lambda = 2$ and aspect ratio 10. The results presented in this figure for CLT are obtained by discretizing the plate into 50 layers through its thickness. No discretization is used for the present method.

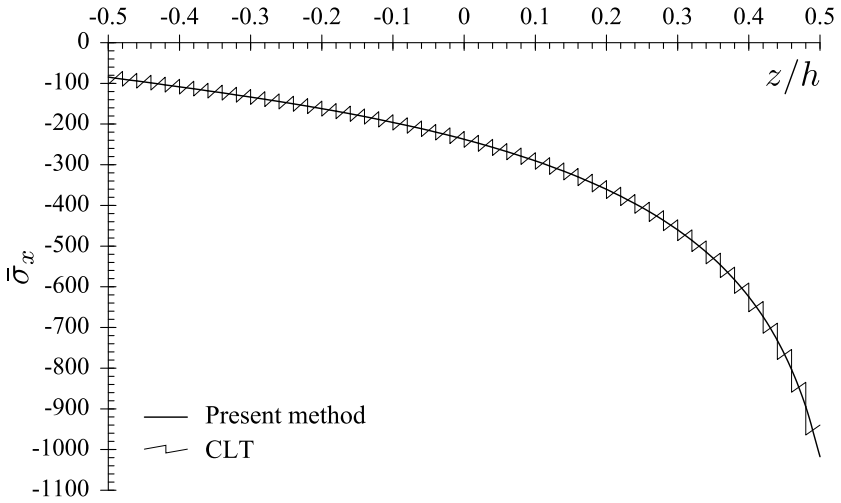

Figure 12: Comparison between in-plane stress predictions of present method and CLT ($a/h = 10$, $\lambda = 2$)

It is apparent from Fig. 12 that the stresses predicted using the two approaches follow the same trend. This is expected since both approaches share very similar stiffness and loading matrices. The assumption used in CLT of constant material properties within each layer, however, means that a discontinuity in material properties occurs at every interface between layers. A corresponding stress discontinuity consequently arises which is the cause of the zig-zag effect

visible in Fig. 12. The stress predicted by the present method, however, varies smoothly across the complete thickness of the plate because no discretization is required.

4. Conclusion

An extension to CLT is presented for the improved analysis of thin to moderately thick functionally graded plates. The formulation accommodates any through-thickness variation in orthotropic material properties, hygrothermal and piezoelectric loading. This is achieved by using polynomial series to approximate the exact variation in these parameters. This approach allows the resulting mathematical problem to be explicitly formulated. Validation problems demonstrate that the method has sufficient accuracy for many practical engineering applications.

References

[1] J.R. Cavanagh, K.R. Cross, R.L. Newman, and W.C. Spicer. The graded thermal barrier - A new approach for turbine engine cooling. In *Proceedings of the Thirteenth U.S. Structural Dynamics and Materials Conference*, page 1, 1972.

[2] M. Koizumi. FGM activities in Japan. *Composites Part B: Engineering*, 28(1-2):1–4, 1997.

[3] U. Schulz, M. Peters, Fr.-W. Bach, and G. Tegeder. Graded coatings for thermal, wear and corrosion barriers. *Materials Science and Engineering A*, 362(1-2):61–80, 2003.

[4] Z.H. Melgarejo, O.M. Suarez, and K. Sridharan. Wear resistance of a functionally-graded aluminum matrix composite. *Scripta Materialia*, 55(1 SPEC ISS):95–98, 2006.

[5] L. Prchlik, S. Sampath, J. Gutleber, G. Bancke, and A.W. Ruff. Friction and wear properties of WC-Co and Mo-Mo_2C based functionally graded materials. *Wear*, 249(12):1103–1115, 2001.

[6] K. Miyoshi, B. Pohlchuck, K.W. Street, J.S. Zabinski, J.H. Sanders, A.A. Voevodin, and R.L.C. Wu. Sliding wear and fretting wear of diamondlike carbon-based, functionally graded nanocomposite coatings. *Wear*, 225-229(I):65–73, 1999.

[7] M. Kemal Apalak and R. Gunes. Investigation of elastic stresses in an adhesively bonded single lap joint with functionally graded adherends in tension. *Composite Structures*, 70(4):444–467, 2005.

[8] Y.Y. Ying and D. Munz. Reduction of residual stresses in a two dissimilar materials joint by using a functionally graded material. In *Composites and Functionally Graded Materials*, pages 37–43. American Society of Mechanical Engineers, Materials Division, 1997.

[9] H. Guo, K.A. Khor, Y.C. Boey, and X. Miao. Laminated and functionally graded hydroxyapatite/yttria stabilized tetragonal zirconia composites fabricated by spark plasma sintering. *Biomaterials*, 24(4):667–675, 2003.

[10] Y.H. Hsu, I.G. Turner, and A.W. Miles. Fabrication of porous bioceramics with porosity gradients similar to the bimodal structure of cortical and cancellous bone. *Journal of Materials Science: Materials in Medicine*, 18(12):2251–2256, 2007.

[11] H.S. Hedia. Design of functionally graded dental implant in the presence of cancellous bone. *Journal of Biomedical Materials Research - Part B Applied Biomaterials*, 75(1):74–80, 2005.

[12] K. Kato, M. Kurimoto, H. Shumiya, H. Adachi, S. Sakuma, and H. Okubo. Application of functionally graded material for solid insulator in gaseous insulation system. *IEEE Transactions on Dielectrics and Electrical Insulation*, 13(2):362–371, 2006.

[13] J.N. Reddy and Z.-Q. Cheng. Three-dimensional thermomechanical deformations of functionally graded rectangular plates. *European Journal of Mechanics, A/Solids*, 20(5):841–855, 2001.

[14] M. Kashtalyan. Three-dimensional elasticity solution for bending of functionally graded rectangular plates. *European Journal of Mechanics, A/Solids*, 23(5):853–864, 2004.

[15] M. Kashtalyan and M. Menshykova. Three-dimensional elasticity solution for sandwich panels with a functionally graded core. *Composite Structures*, 87(1):36–43, 2009.

[16] A.M. Zenkour. Benchmark trigonometric and 3-D elasticity solutions for an exponentially graded thick rectangular plate. *Archive of Applied Mechanics*, 77(4):197–214, 2007.

[17] S.S. Vel and R.C. Batra. Exact solution for thermoelastic deformations of functionally graded thick rectangular plates. *AIAA Journal*, 40(7):1421–1433, 2002.

[18] S.S. Vel and R.C. Batra. Three-dimensional analysis of transient thermal stresses in functionally graded plates. *International Journal of Solids and Structures*, 40(25):7181–7196, 2003.

[19] S.S. Vel and R.C. Batra. Three-dimensional exact solution for the vibration of functionally graded rectangular plates. *Journal of Sound and Vibration*, 272(3-5):703–730, 2004.

[20] E. Pan. Exact solution for functionally graded anisotropic elastic composite laminates. *Journal of Composite Materials*, 37(21):1903–1920, 2003.

[21] A. Alibeigloo. Exact solution for thermo-elastic response of functionally graded rectangular plates. *Composite Structures*, 92(1):113–121, 2010.

[22] E. Carrera. A priori vs. a posteriori evaluation of transverse stresses in multilayered orthotropic plates. *Composite Structures*, 48(4):245–260, 2000.

[23] E. Carrera. An assessment of mixed and classical theories on global and local response of multilayered orthotropic plates. *Composite Structures*, 50(2):183–198, 2000.

[24] J.N. Reddy. Analysis of functionally graded plates. *International Journal for Numerical Methods in Engineering*, 47(1):663–684, 2000.

[25] J.N. Reddy, C.M. Wang, and S. Kitipornchai. Axisymmetric bending of functionally graded circular and annular plates. *European Journal of Mechanics, A/Solids*, 18(2):185–199, 1999.

[26] A.J.M. Ferreira, R.C. Batra, C.M.C. Roque, L.F. Qian, and R.M.N. Jorge. Natural frequencies of functionally graded plates by a meshless method. *Composite Structures*, 75(1-4):593–600, 2006.

[27] T.-K. Nguyen, K. Sab, and G. Bonnet. First-order shear deformation plate models for functionally graded materials. *Composite Structures*, 83(1):25–36, 2008.

[28] A.J.M. Ferreira, R.C. Batra, C.M.C. Roque, L.F. Qian, and P.A.L.S. Martins. Static analysis of functionally graded plates using third-order shear deformation theory and a meshless method. *Composite Structures*, 69(4):449–457, 2005.

[29] A.J.M. Ferreira, C.M.C. Roque, R.M.N. Jorge, G.E. Fasshauer, and R.C. Batra. Analysis of functionally graded plates by a robust meshless method. *Mechanics of Advanced Materials and Structures*, 14(8):577–587, 2007.

[30] L.F. Qian and R.C. Batra. Transient thermoelastic deformations of a thick functionally graded plate. *Journal of Thermal Stresses*, 27(8):705–740, 2004.

[31] A.M. Zenkour. Generalized shear deformation theory for bending analysis of functionally graded plates. *Applied Mathematical Modelling*, 30(1):67–84, 2006.

[32] A.M. Zenkour. A comprehensive analysis of functionally graded sandwich plates: Part 1-Deflection and stresses. *International Journal of Solids and Structures*, 42(18-19):5224–5242, 2005.

[33] A.M. Zenkour and N.A. Alghamdi. Thermomechanical bending response of functionally graded nonsymmetric sandwich plates. *Journal of Sandwich Structures and Materials*, 12(1):7–46, 2010.

[34] S. Kapuria, M. Bhattacharyya, and A.N. Kumar. Assessment of coupled 1D models for hybrid piezoelectric layered functionally graded beams. *Composite Structures*, 72(4):455–468, 2006.

[35] S. Kapuria, M. Bhattacharyya, and A.N. Kumar. Bending and free vibration response of layered functionally graded beams: A theoretical model and its experimental validation. *Composite Structures*, 82(3):390–402, 2008.

[36] S. Kapuria, M. Bhattacharyya, and A.N. Kumar. Theoretical modeling and experimental validation of thermal response of metal-ceramic functionally graded beams. *Journal of Thermal Stresses*, 31(8):759–787, 2008.

[37] U. Icardi and L. Ferrero. Optimisation of sandwich panels with functionally graded core and faces. *Composites Science and Technology*, 69(5):575–585, 2009.

[38] E. Carrera. An assessment of mixed and classical theories for the thermal stress analysis of orthotropic multilayered plates. *Journal of Thermal Stresses*, 23(9):797–831, 2000.

[39] P.F. Pai and A.N. Palazotto. Two-dimensional sublamination theory for analysis of functionally graded plates. *Journal of Sound and Vibration*, 308(1-2):164–189, 2007.

[40] E. Carrera. A class of two-dimensional theories for anisotropic multilayered plates analysis. *Accademia delle Scienze di Torino*, 49-87:1–39, 1995.

[41] E. Carrera. Theories and finite elements for multilayered plates and shells: A unified compact formulation with numerical assessment and benchmarking. *Archives of Computational Methods in Engineering*, 10(3):215–296, 2003.

[42] E. Carrera and A. Ciuffreda. A unified formulation to assess theories of multilayered plates for various bending problems. *Composite Structures*, 69(3):271–293, 2005.

[43] S. Brischetto and E. Carrera. Advanced mixed theories for bending analysis of functionally graded plates. *Computers and Structures*, 2008. Article in Press doi:10.1016/j.compstruc.2008.04.004.

[44] E. Carrera, S. Brischetto, and A. Robaldo. Variable kinematic model for the analysis of functionally graded material plates. *AIAA Journal*, 46(1):194–203, 2008.

[45] S. Brischetto. Classical and mixed advanced models for sandwich plates embedding functionally graded cores. *Journal of Mechanics of Materials and Structures*, 4(1):13–33, 2009.

[46] S. Brischetto, R. Leetsch, E. Carrera, T. Wallmersperger, and B. Krplin. Thermo-mechanical bending of functionally graded plates. *Journal of Thermal Stresses*, 31(3):286–308, 2008.

[47] S. Brischetto and E. Carrera. Refined 2D models for the analysis of functionally graded piezoelectric plates. *Journal of Intelligent Material Systems and Structures*, 20(15):1783–1797, 2009.

[48] E. Carrera and A. Ciuffreda. Closed-form solutions to assess multilayered-plate theories for various thermal stress problems. *Journal of Thermal Stresses*, 27(11):1001–1031, 2004.

[49] A.E. Giannakopoulos, S. Suresh, M. Finot, and M. Olsson. Elastoplastic analysis of thermal cycling: Layered materials with compositional gradients. *Acta Metallurgica Et Materialia*, 43(4):1335–1354, 1995.

[50] C.H. Hsueh and S. Lee. Modeling of elastic thermal stresses in two materials joined by a graded layer. *Composites Part B: Engineering*, 34(8):747–752, 2003.

[51] T.L. Becker Jr., R.M. Cannon, and R.O. Ritchie. An approximate method for residual stress calculation in functionally graded materials. *Mechanics of Materials*, 32(2):85–97, 2000.

[52] K.S. Ravichandran. Thermal residual stresses in a functionally graded material system. *Materials Science and Engineering A*, 201(1-2):269–276, 1995.

[53] M. Finot, S. Suresh, C. Bull, and S. Sampath. Curvature changes during thermal cycling of a compositionally graded Ni-Al_2O_3 multi-layered material. *Materials Science and Engineering A*, 205(1-2):59–71, 1996.

[54] J.R. Cho and J.T. Oden. Functionally graded material: A parametric study on thermal-stress characteristics using the Crank-Nicolson-Galerkin scheme. *Computer Methods in Applied Mechanics and Engineering*, 188(1):17–38, 2000.

[55] H. Tsukamoto. Analytical method of inelastic thermal stresses in a functionally graded material plate by a combination of micro- and macromechanical approaches. *Composites Part B: Engineering*, 34(6):561–568, 2003.

[56] L.L. Shaw. Thermal residual stresses in plates and coatings composed of multi-layered and functionally graded materials. *Composites Part B: Engineering*, 29(3):199–210, 1998.

[57] M. Taya, A. Almajid, M. Dunn, and H. Takahashi. Design of bimorph piezocomposite actuators with functionally graded microstructure. *Sensors and Actuators, A: Physical*, 107(3):248–260, 2003.

[58] A. Almajid, M. Taya, and S. Hudnut. Analysis of out-of-plane displacement and stress field in a piezocomposite plate with functionally graded mi-

crostructure. *International Journal of Solids and Structures*, 38(19):3377–3391, 2001.

[59] A. Almajid and M. Taya. 2D-elasticity analysis of FGM piezo-laminates under cylindrical bending. *Journal of Intelligent Material Systems and Structures*, 12(5):341–351, 2002.

[60] C.T. Herakovich. *Mechanics of Fibrous Composites*. John Wiley & Sons, Inc., 1998.

[61] A.K. Kaw. *Mechanics of Composite Materials*. CRC Press, Boca Raton, FL, 2nd edition, 2006.

[62] S Adachi. *GaAs and Related Materials : Bulk Semiconducting and Superlattice Properties*. World Scientific Publishing, Singapore, 1994.

[63] S.V. Gopinathan, V.V. Varadan, and V.K. Varadan. Review and critique of theories for piezoelectric laminates. *Smart Materials and Structures*, 9(1):24–48, 2000.